Study on Thermal Expansion in Injection-Molded Isotactic Polypropylene and Thermoplastic Elastomer Blends

Michio Ono,[1]* Ken Nakajima,[2] Toshio Nishi[2]

[1]*SunAllomer Ltd., Kawasaki Development Center, 2-3-2 Yako-cho, Kawasaki-ku, Kawasaki, Kanagawa 210-0863, Japan*
[2]*Department of Organic and Polymeric Materials, Tokyo Institute of Technology, Ookayama, Meguro-ku, Tokyo 152-8552, Japan*

Received 12 March 2007; accepted 27 May 2007
DOI 10.1002/app.27192
Published online 26 November 2007 in Wiley InterScience (www.interscience.wiley.com).

ABSTRACT: The linear thermal expansion coefficients (CLTEs) along flow direction (FD) for the injection-molded blends composed of isotactic polypropylene (iPP) and various ethylenic thermoplastic elastomers (TPEs) were investigated using a thermo-mechanical analyzer. The iPP/TPE blends with higher comonomer contents in the TPE showed extremely low CLTE. TEM observation revealed that the array of the TPE whose MFR was adjusted to be higher than the iPP matrix was in lamella-like sheet stacked normal to normal direction (ND) with being elongated along both FD and transverse-to-flow direction. At higher magnification of TEM, the iPP lamellae in the blend with higher comonomer contents in the TPE deeply penetrated into the TPE phase as a consequence of the faster iPP crystallization before the completion of the phase-separation. Hence, the location of the iPP amorphous chains would change depending on the comonomer contents in the TPE; in the case of the iPP/TPE blend with higher comonomer contents, large amount of the iPP amorphous chains would be trapped inside the TPE phase because of incomplete phase-separation arrested by faster crystallization. Therefore, the extremely low CLTE for the iPP/TPE blend with higher comonomer contents was accounted for by the simultaneous suppression of the thermal expansions from both the TPE phase and the iPP amorphous chains trapped inside the TPE by rigid iPP crystalline lamellae connecting in parallel with the TPE phase. J Appl Polym Sci 107: 2930–2943, 2008

Key words: injection molding; poly(propylene); TEM; phase-separation

INTRODUCTION

Isotactic polypropylene (iPP)/thermoplastic elastomer (TPE) blends have been widely used as injection-molded automobile exterior parts, in particular, bumper fascia because of their good price/performance ratio, excellent processability, and good wetherability.[1] Nowadays, the bumper fascia has been regarded as a part of exterior panels by being integrated with other exterior parts such as air-intakes and fender panels. Hence, appearance quality as a design part, in addition to a role of an impact absorber for the conventional safety parts, has been also required for the recent bumper fascia.

The exterior parts including bumper fascias are usually subject to severe thermal conditions ranging from −50 to 80°C. It has been well-known that the iPP has a high thermal expansion (∼ 14–15 (10^{-5}/°C)),[2] when compared with metals (∼ 10^{-6}/°C)[3] and other amorphous polymers (∼ 7.0–9.0 (10^{-5}/°C)).[2] Because of this, a gap or deformation resulting from the dimensional mismatch between the iPP-based bumper fascias and the integrated exterior parts comprising metal or other polymers may arise with temperature change, leading to deterioration of the appearance quality.

One of the conventional ways to solve the issue is loading inorganic filler with high aspect ratio (talc, glass fiber, or mica) into iPP, and suppressing bulk expansion by a simple mechanical constraint.[4–7] However, incorporating the inorganic fillers has brought about the weight increase of the molded articles containing higher density inorganic fillers. In addition, the filler-reinforced PP is not appropriate for the environmentally-friendly material because of ash remained after combustion.

Recently, a new technology to control the thermal expansion of the injection-molded filler-less iPP-based alloy was proposed by us[8–10] and Wu et al.,[11] in which the TPE having well-controlled viscosity was employed as an ingredient instead of fillers. In this technology, the adjustment of the thermal expansion was achieved by controlling anisotropy in the linear thermal expansion coefficients (CLTE) along each direction of the injection-molded article not by suppressing the bulk expansion; extremely low CLTE along both flow direction (FD) and

**Present address:* Dow Japan Development Center, Dow Chemical Japan Ltd., 8-1 Ukishima-cho, Kawasaki-ku, Kawasaki-shi, Kanagawa-ken, 210-0862, Japan.
Correspondence to: M. Ono (michio_ono@sunallomer.co.jp).

Journal of Applied Polymer Science, Vol. 107, 2930–2943 (2008)

TABLE I
Characteristics of Raw Materials

Polymer type	Designation	Co-unit content (nominal) wt %	MFR at 230°C dg/min	T_m (°C)	Flexure modulus (R.T.) MPa
Isotactic PP	iPP	–	2.8	166	1,650
Polyethylene (PE)	HD[a]	–	8.1	135	1,300
	LD[b]	–	10	113	140
Poly(ethylene-*co*-octene) (EOR)	EOR9	9.0	6.3	103	110
	EOR24	24	8.9	60	12
	EOR30	30	2.8	33	3.5
Poly(ethylene-*co*-butene) (EBR)	EBR5	5.0	16	120	160
	EBR17	17	5.9	85	20
	EBR20	20	6.0	68	14
	EBR32	32	6.8	35	10
Poly(ethylene-co-propylene) (EPR)	EPR30	30	1.0	43	No date (<3.0)
	EPR57	57	0.86	No melting peak	No data (<3.0)

[a] High density polyethylene.
[b] Low density polyethylene.

transverse-to-flow direction (TD) while extremely high along normal direction (ND).

In the previous papers,[9,10] we clarified that the preferential thermal expansion along ND was somewhat accounted for by the lamella-sheet morphology in the TPE domains connecting in parallel with the base iPP, the exclusive *b*-axis orientation of the iPP crystal along ND, the aspect ratio of the lamella-sheet arrays in the TPE domains and the retraction due to the interfacial tension from the molten elastomer. However, suppressing CLTE along FD, which is much more important for practical use, could not be explained only by these factors.

In this study, we prepared some injection-molded iPP/TPE blends having various types and contents of comonomer in the TPE, and investigated influencing factors for inducing such an extremely low CLTE in FD from the view point of the location of the iPP amorphous chains.

EXPERIMENTAL

Materials and sample preparation

Isotactic polypropylene (iPP) having 165°C of melting temperature, 98.5% of mmmm pentad sequences by ^{13}C NMR, and 2.8 dg/min of melt low rate (MFR) at 230°C was kindly donated from SunAllomer. We chose four types of olefinic polymer combining with the iPP, poly(ethylene-*co*-propylene) rubber (EPR), poly(ethylene-*co*-butene) rubber (EBR), poly(ethylene-*co*-octene) rubber (EOR), and polyethylene (PE). Their general characteristics were presented in Table I. The MFRs of them were higher than that of the matrix iPP in order to adjust the morphology of the TPE domain to be sheet array (discussed later). The designation of the polymers used in this study was based on the polymer type and the comonomer content; for instance, EOR containing 9.0 wt % of 1-octene as a comonomer was designated as EOR9.

The binary blend with 70/30 (v/v) composition of iPP/TPE was prepared by being melt-blended with a corotating twin screw extruder with 52 of L/D (TEX30α; JSW) under 180°C of cylinder setting temperatures. The blend was injection-molded to obtain a slab-shaped specimen, 125 (length) by 20 (width) by 3.0 (thickness) mm^3 using an injection machine (α100C; FUNAC) under 200°C of cylinder setting temperatures, 40°C of a mold temperature, and 40°mm/s of an injection rate. The definition of the directions and cross-sections were designated in Figure 1. The specimens obtained were annealed at 100°C for 24 h prior to use to remove residual stress developing during the injection-molding.

The characteristic and sample designation of each resulting blend was presented in Table II. Thermal properties of iPP crystalline region in the blends, the heat of fusion (ΔH_c) and the melting temperature (T_m) were measured with a differential scanning calorimetry (DSC) (DSC-7, Perkin-Elmer) under a nitrogen atmosphere. The samples cut from the injection-molded slabs were. sealed in an aluminum pan was

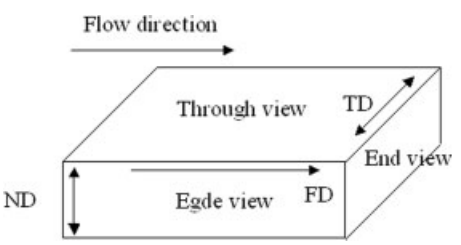

Figure 1 Definition of the direction, FD for flow direction, TD for transverse to flow direction, and ND for normal to flow direction as well as the cross-section, edge-view parallel to FD, end-view parallel to TD and through view normal to ND.

TABLE II
Characteristics of ipp-TPE Blends

Sample designation	Polymer type	T_m (°C)	MFR ratio; TPE/iPP	Flexural modulus ratio; TPE/iPP	ΔH_c (J/g)	X_c (%)
iPP	Isotactic PP	166	–	–	103	49
iPP-HD	PE	164	2.9	0.78	68	46
iPP-LD		165	5.7	0.085	68	46
iPP-EOR9	Poly(ethylene-*co*-octene) (EOR)	165	2.3	0.062	68	46
iPP-EOR24		164	3.2	0.036	70	48
iPP-EOR30		166	1.0	0.020	72	49
iPP-EBR5	Poly(ethylene-*co*-butene) (EBR)	165	5.7	0.073	70	48
iPP-EBR17		166	2.1	0.052	68	46
iPP-EBR20		166	2.1	0.041	69	47
iPP-EBR32		164	2.4	0.021	67	46
iPP-EPR30	Poly(ethylene-*co*-propylene) (EPR)	164	0.36	< 0.0020	69	47
iPP-EPR57		165	0.31	< 0.0020	70	48

firstly heated to 230°C, gradually cooled to −20°C at a rate of 10°C/min and then heated to 230°C at a rate of 10°C/min. The ΔH_c and the T_m were determined based on the second heating thermogram. The crystallinity of the iPP crystal, X_c was obtained by dividing the ΔH_c by the one corresponding to the perfect crystalline iPP, 209 J/g.[12]

CLTE evaluation

The specimen for the CLTE measurement was punched out from the central part of the slab. The size of the specimen was 12.0 (height) by 5.0 (length) by 3.0 (width) mm^3, in which the ''height'' direction coincided with the FD (measured direction). The CLTE measurement was performed in a compression mode under a load of 0.039 N using a thermal mechanical analyzer (TMA) (MTS9000; Sinku Riko) at a heating rate of 4.0°C/min. The CLTE was monitored ranging from 0 to 100°C. The average CLTE (α^{obs}) on a given temperature range was defined as eq. (1).

$$\alpha^{obs} = \frac{1}{L}\frac{L_2 - L_1}{T_2 - T_1} \quad (1)$$

where L, L_1, and L_2 are the reference length measured at 23°C, the length at T_1 (0°C in this work), and the length at T_2 (100°C in this work), respectively.

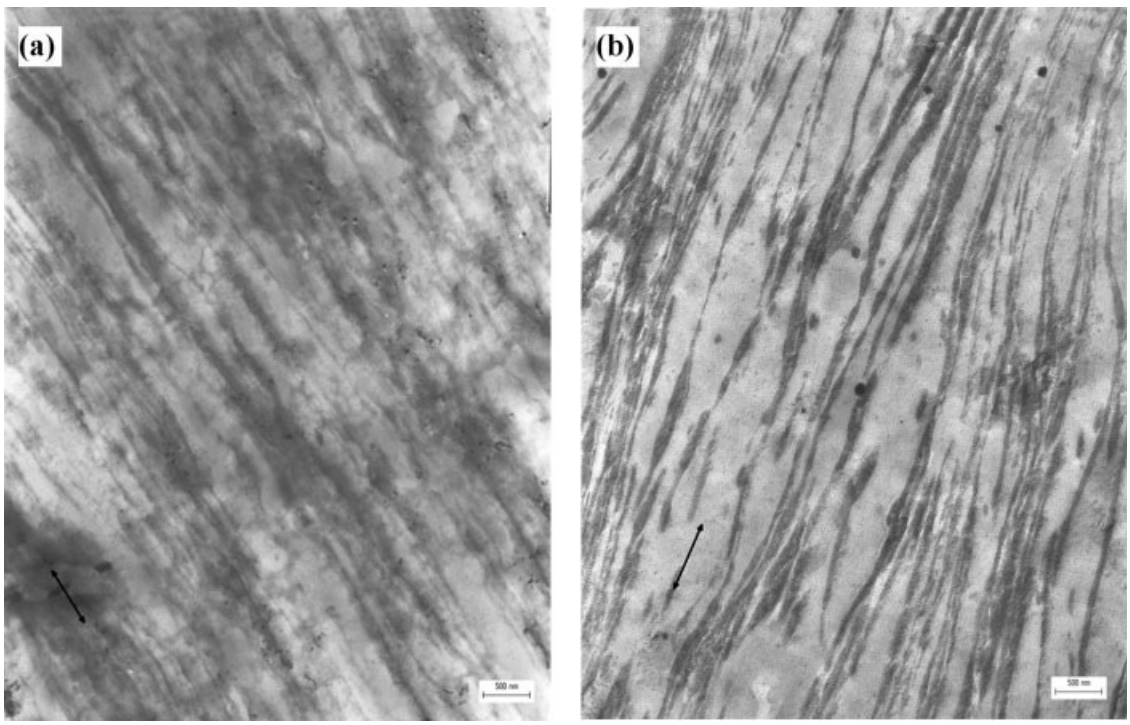

Figure 2 TEM photographs from the edge-view of iPP-PE blends; (a) iPP-HDPE and (b) iPP-LDPE, respectively. The arrow indicates the FD.

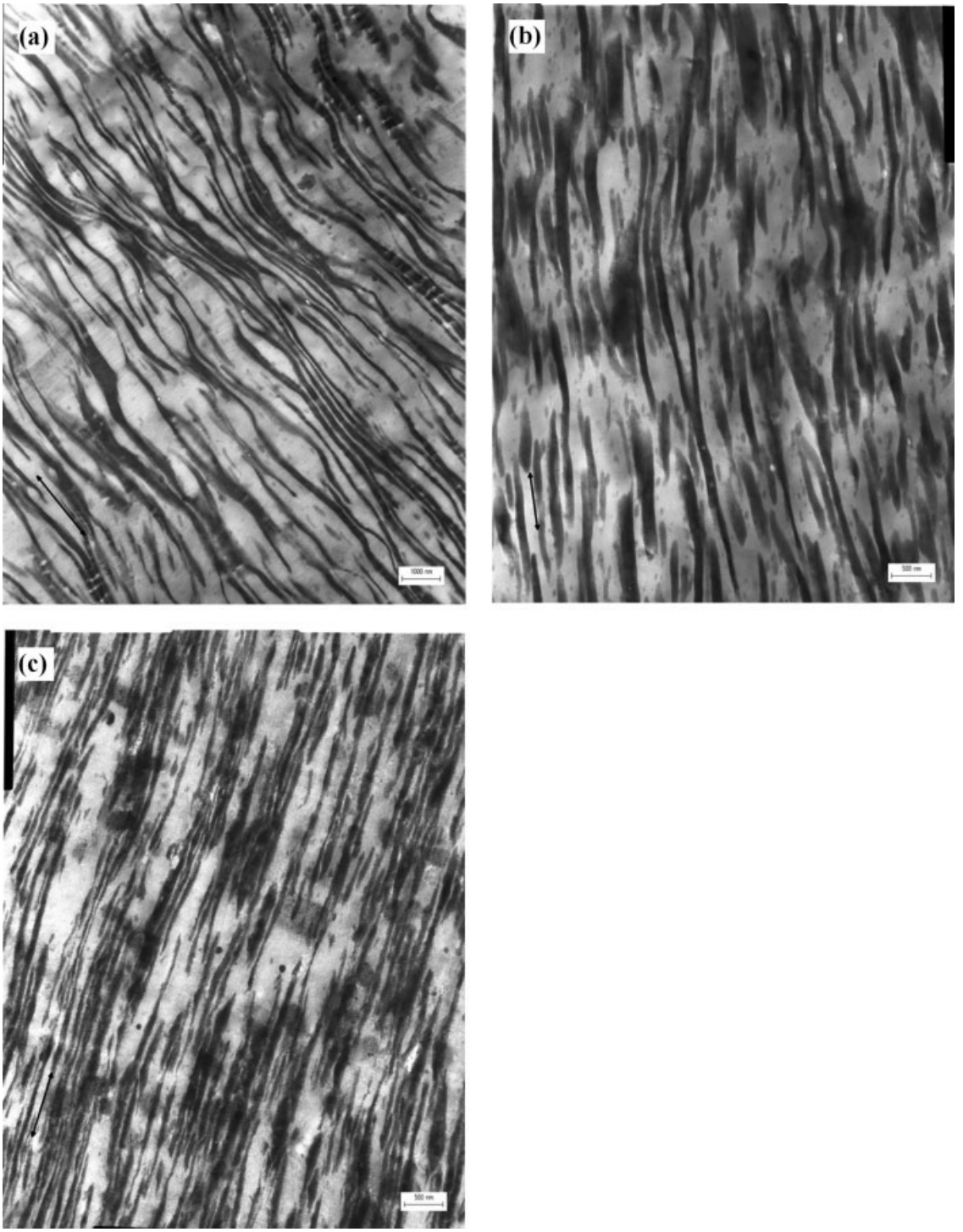

Figure 3 TEM photographs from the edge-view of iPP-EOR blends; (a) iPP-EOR9, (b) iPP-EOR24, and (c) iPP-EOR30, respectively. The arrow indicates the FD.

Morphology observation

The morphologies of the edge- and end-view were observed using a transmission electron microscopy (TEM) (JEM1200EX; JEOL) operated at 120 kV of an accelerating voltage. An ultra-thin section (thickness; 70–80 nm) microtomed at −100°C was taken from the core layer of the injection specimen after being stained with RuO_4 vapor at 40°C for 5 h.

PP amorphous orientation by polarized light optical microscopy

The orientation function f_{am}^{FD} of the iPP amorphous region in FD was determined from the birefringence

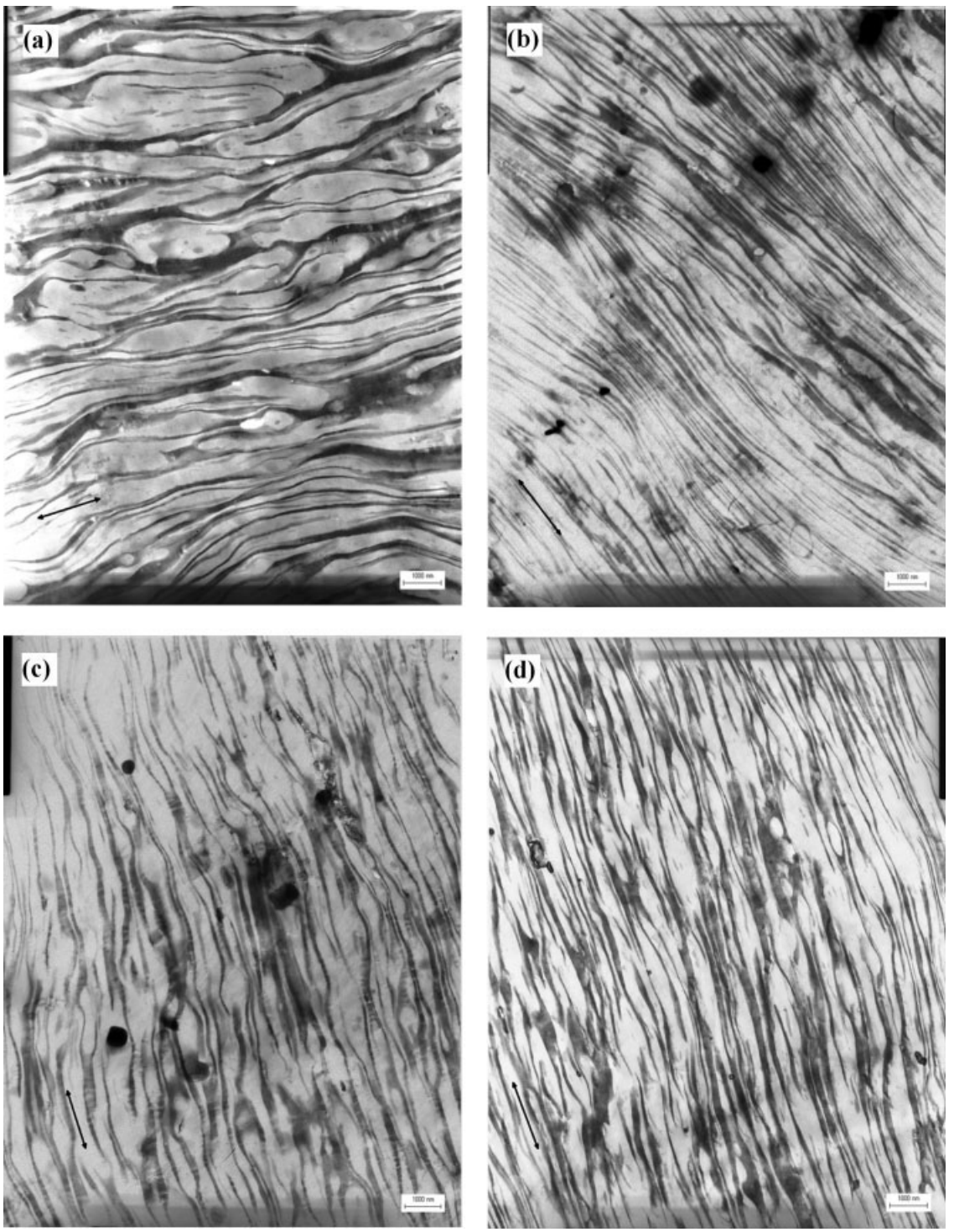

Figure 4 TEM photographs from the edge-view of iPP-EBR blends; (a) iPP-EBR5, (b) iPP-EBR17, (c) iPP-EBR20, and (d) iPP-EOR32, respectively. The arrow indicates the FD.

(Δn) (measured), degree of crystallinity (X_c), and *c*-axis orientation function (f_c^{FD}) in the FD obtained by the X-ray pole figure[9] using

$$f_{\mathrm{am}}^{\mathrm{FD}} = \frac{\Delta n - \Delta n_c^0 X_c f_c^{\mathrm{FD}}}{\Delta n_{\mathrm{am}}^0 (1 - X_c)} \quad (2)$$

where Δn_c^0 and Δn_{am}^0 were the intrinsic crystal birefringence and the intrinsic amorphous birefringence, 0.0331 and 0.0468, respectively.[13,14]

The Δn was obtained by a polarized light optical microscope (POM) (BLX-40, Olympus Optical) with a Berek compensator. The sample was sliced to

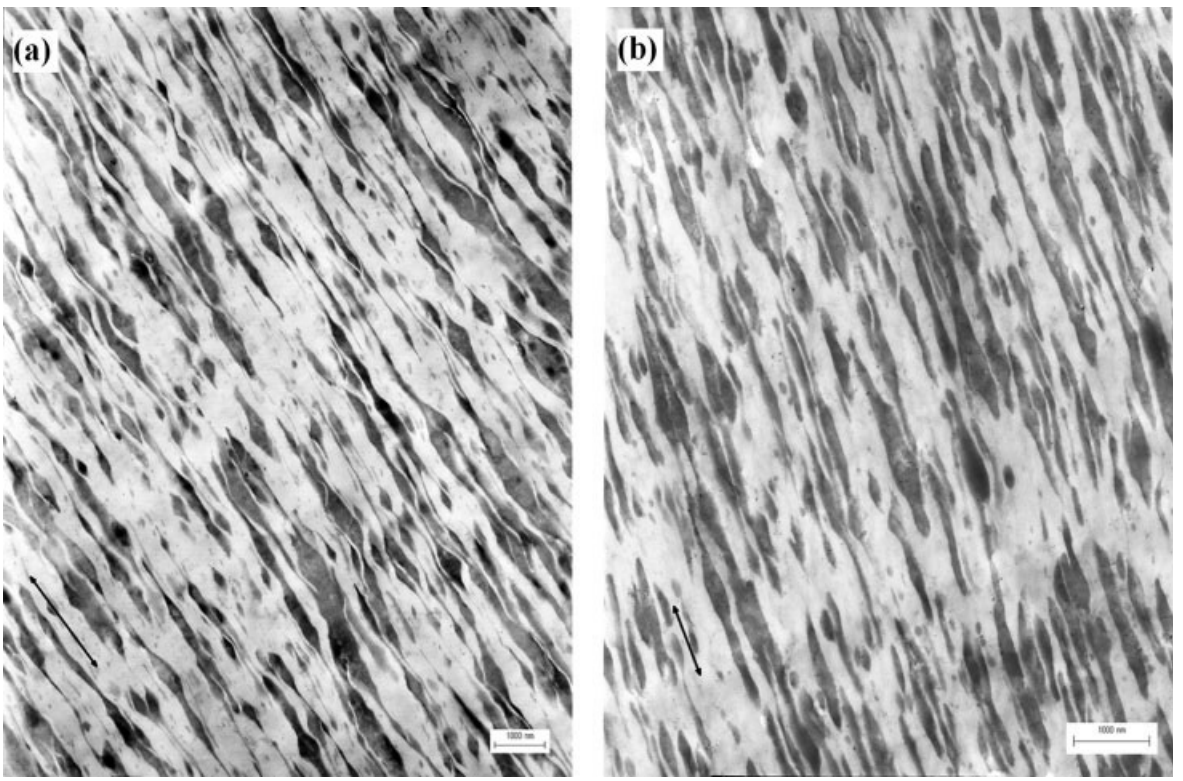

Figure 5 TEM photographs from the edge-view for iPP-EPR blends; (a) iPP-EPR30 and (b) iPP-EPR57, respectively. The arrow indicates the FD.

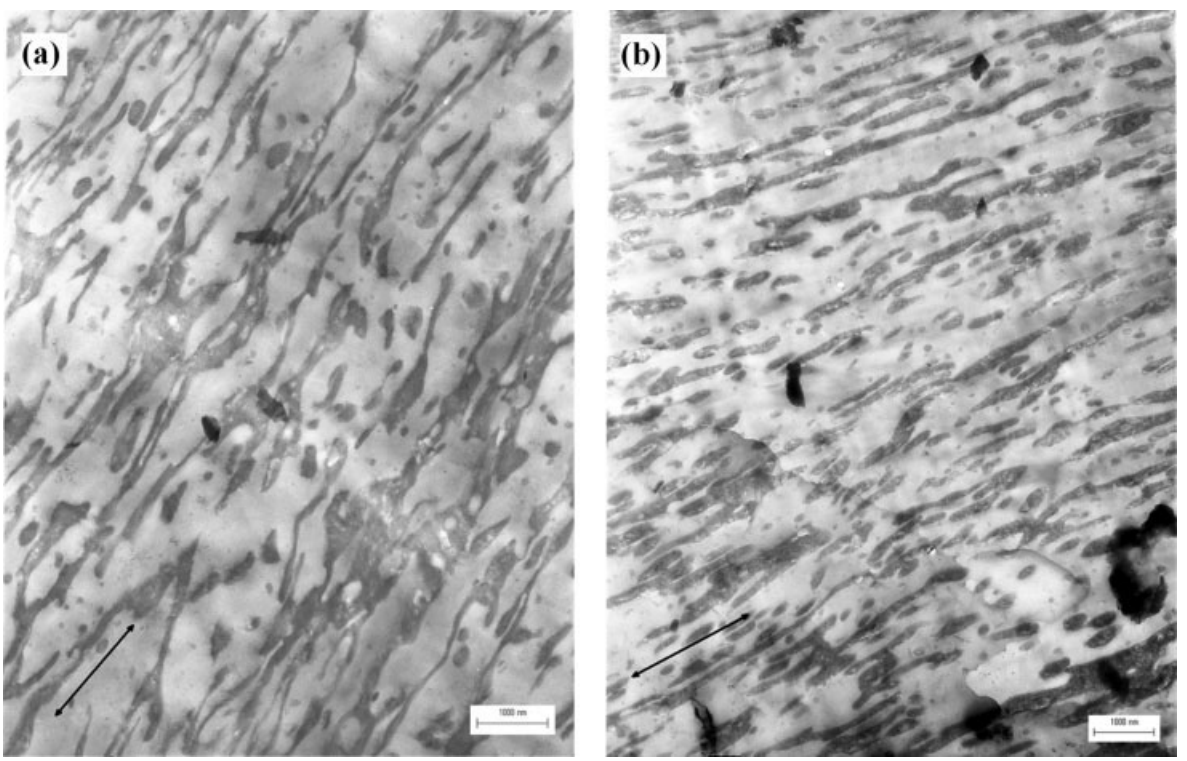

Figure 6 TEM photographs from the end-view for iPP-PE blends; (a) iPP-HDPE and (b) iPP-LDPE, respectively. The arrow indicates the TD.

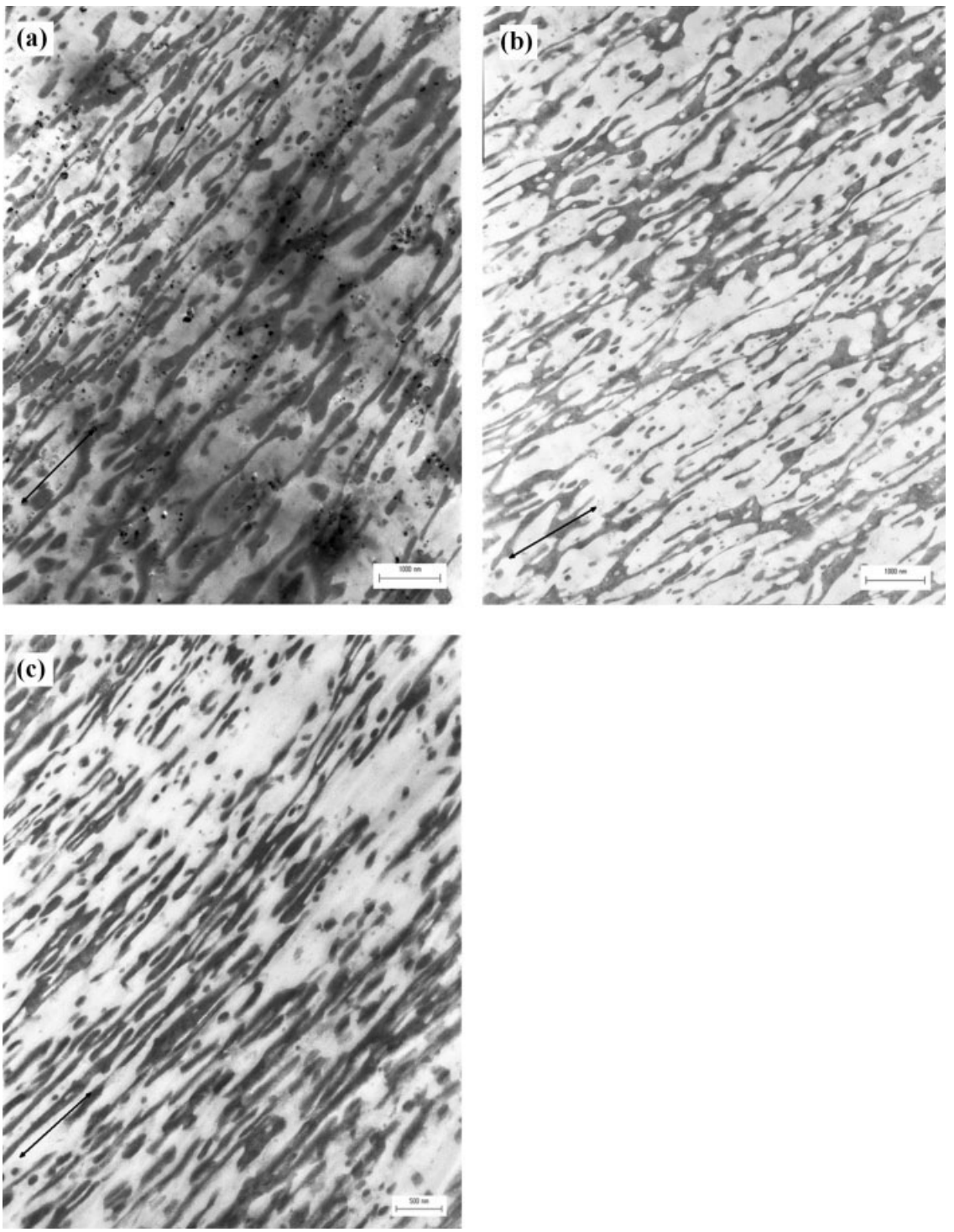

Figure 7 TEM photographs from the end-view of iPP-EOR blends; (a) iPP-EOR9, (b) iPP-EOR24, and (c) iPP-EOR30, respectively. The arrow indicates the TD.

50 μm thickness from the edge view with a razor blade at room temperature.

Dynamic mechanical thermal analysis

The measurements on the linear dynamic mechanical properties were made using a dynamic mechanical thermal analyzer (DMTA) (RSA-III; TA Instruments) on a tensile mode. The rectangular specimens with 30 (length) by 3.0 (width) by 0.4 (thickness) mm^3 were cut out from the slab in such a way that the ''length'' direction, thus the oscillatory strain direction, coincided with the FD. Storage modulus (E'), loss modulus (E''), and loss tangent (tan δ) were monitored ranging from −80 to 140°C at a constant frequency of 1.0 Hz and a heating rate of 4.0°C/min.

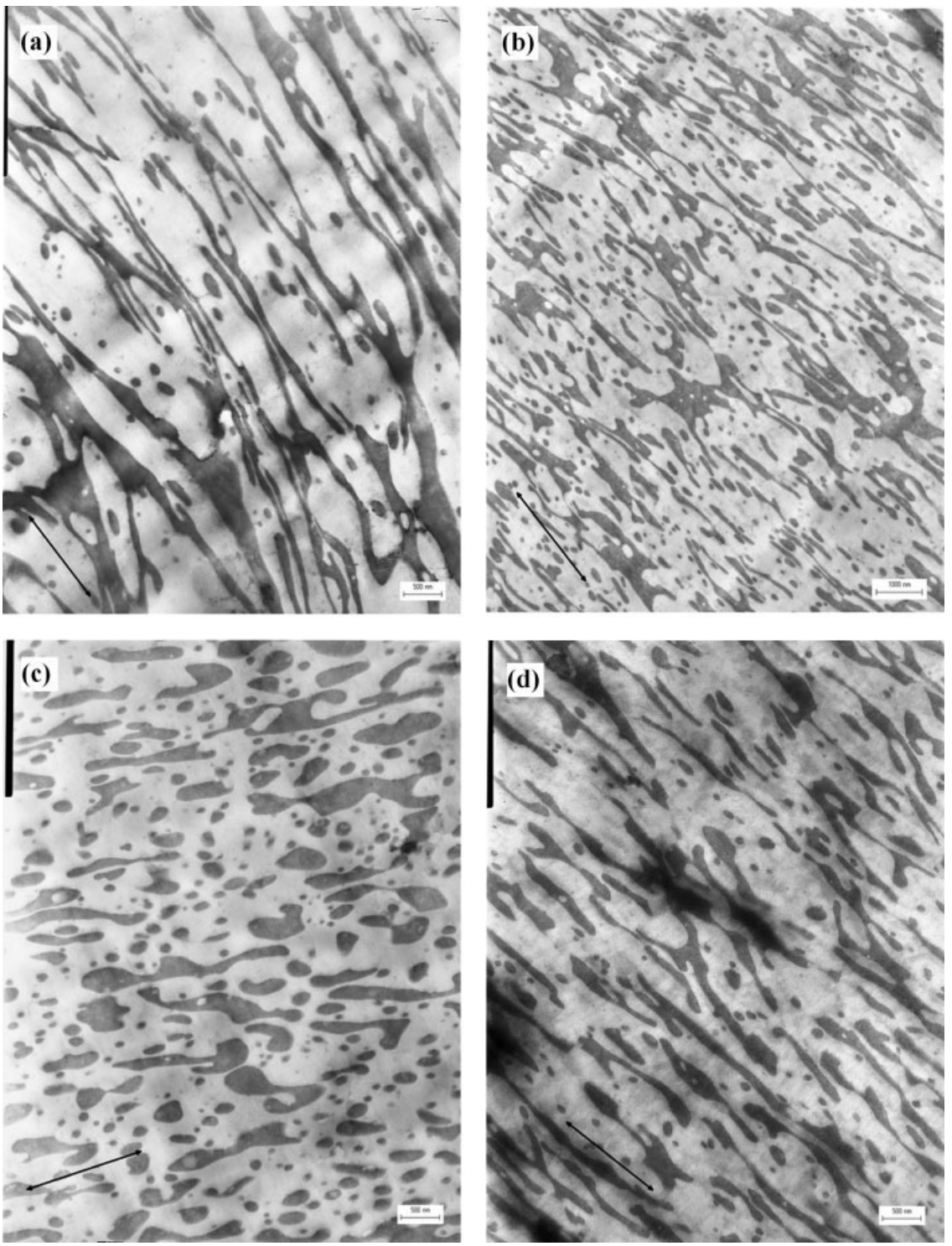

Figure 8 TEM photographs from the end-view of iPP-EBR blends; (a) iPP-EBR5, (b) iPP-EBR17, (c) iPP-EBR20, and (d) iPP-EOR32, respectively. The arrow indicates the TD.

RESULTS

Morphology observation by TEM

Figures 2–5 show the TEM micrographs in the edge-view parallel to FD for the iPP-PE, -EOR, -EBR, and -EPR blend, respectively. The dark regions represent the TPE-rich phases and the bright ones are the iPP-rich phases. In the iPP-PE (Fig. 2), -EOR (Fig. 3), and -EBR (Fig. 4), the TPE-rich phases are highly deformed to FD, thus resulting in long thin fibrils, and form cocontinuous structures with the iPP matrix. In the iPP-EPR blends (Fig. 5), on the other

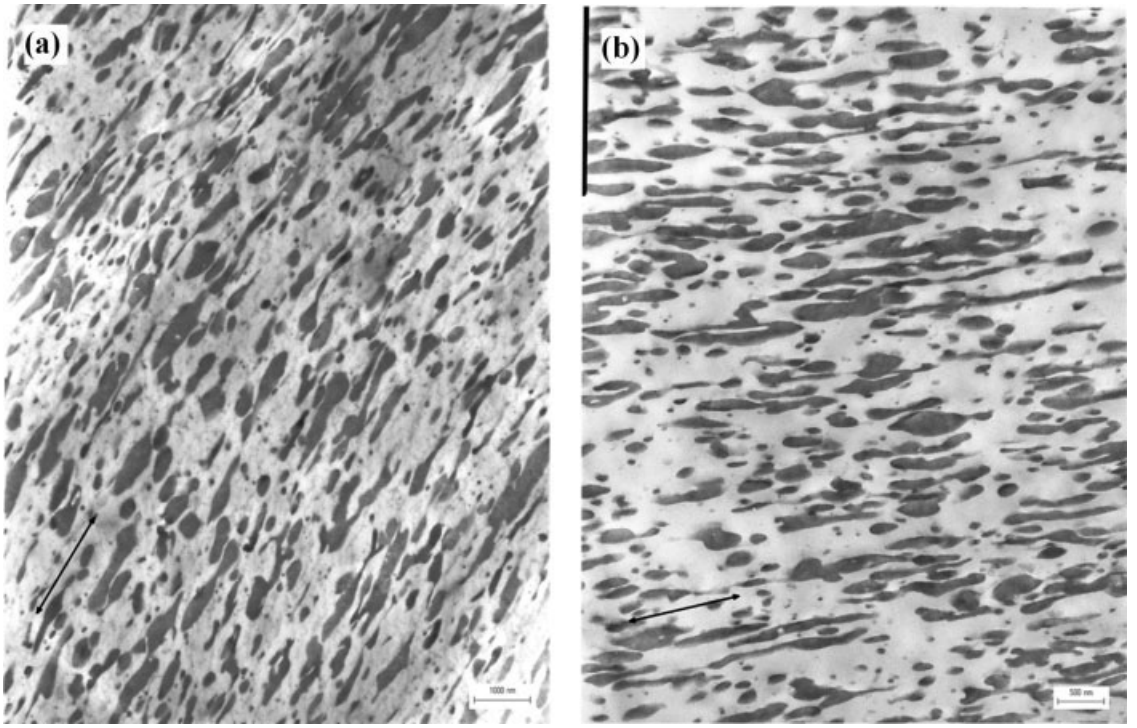

Figure 9 TEM photographs from the edge-view for iPP-EPR blends; (a) iPP-EPR30 and (b) iPP-EPR57, respectively. The arrow indicates the TD.

hand, coarse, short fibrils together with long fibrils are sporadically observed.

For Newtonian fluids, drop-to-fibril transition under a shear was investigated by many researchers.[15–17] They reported that the driving force for the fibril formation was a viscosity ratio of droplet to matrix with being close to or less than unity. The result was applicable for the non-Newtonian fluid such as a polymer–polymer binary blend; in fact, in injection-molded iPP and EPR binary blend, long thin fibril formation was reported when the viscosity ratio (τ) of the dispersed TPE to the iPP matrix was equal to or less than unity under shear flow.[18]

Hence, for the present PE, EOR, and EBR blends, the major factor for the thin fibril formation will be ascribed to the viscosity ratio when considering their MFR ratios are more than unity, i.e. $\tau \leq 1.0$. In the case of the iPP-EPR blends whose MFR ratios are less than unity, i.e., $\tau \geq 1.0$, an incomplete droplet-to-fibril transition would occur, thus resulting in the coarse, short fibrils.

Figures 6–9 show the TEM micrographs from the end view parallel to TD for the iPP-PE, -EOR, EBR, and -EPR, respectively. The long thin fibril formation is also found although some short fibrils and/or droplets resulting from the break-ups of the fibrils are sporadically observed. The fibril break-ups F6-F9

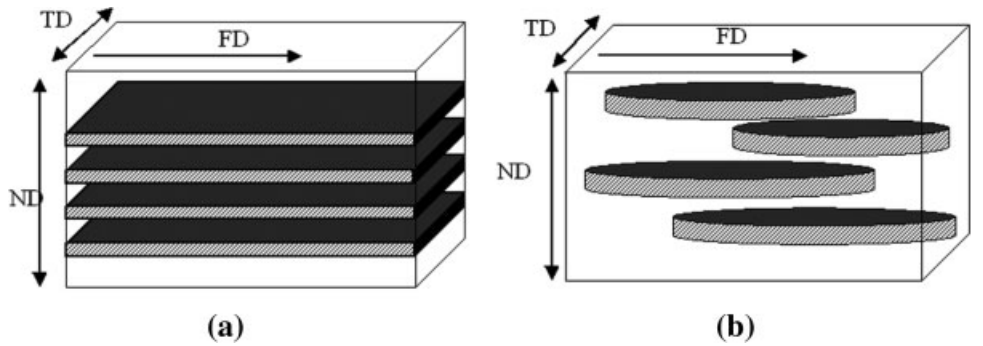

Figure 10 Schematic representation of arrays of TPE domains in the blend; (a) iPP-PE, EO and EB blends with the MFR ratio of TPE to iPP > 1.0, i.e., the melt viscosity ratio of TPE to iPP < 1.0 and (b) iPP-EP blends with the MFR ratio of TPE to iPP < 1.0.

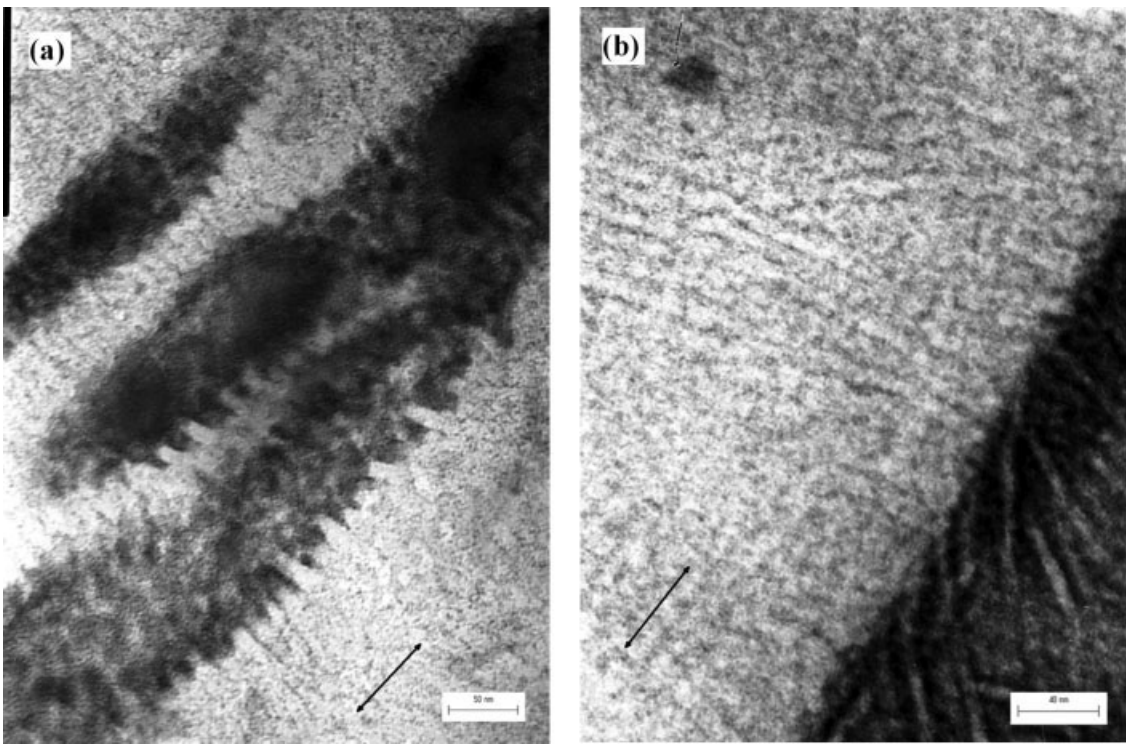

Figure 11 TEM micrographs (edge view) near the interface region between the iPP and the TPE phase for (a) iPP-EO30 and (b) iPP-EO9, respectively.

would be caused by a principal normal stress difference imposed onto the TD, which was reported to be, in general, stronger than the shear stress for the driving force inducing the fibril formation in FD.[19,20]

On the basis of both the edge- and end-view observation, the arrays of the TPE domains are assumed to be in the lamella-like sheets stacked normal to ND for the iPP-PE, -EOR, and -EBR blends, and in the ellipsoidal slab for the iPP-EPR blends. They are schematically illustrated in Figure 10.

Figure 11(a,b) show the TEM micrographs at high magnification for the iPP-EOR30 (higher comonomer contents) and iPP-EOR9 (lower comonomer contents), which can provide the information about the iPP crystal lamellae morphology near the interface region between the TPE phase and the iPP matrix depending on the comonomer contents. In the case of the iPP-EOR30 [Fig. 11(a)], the iPP crystal lamellae deeply penetrate into the deformed EOR phase perpendicularly, which is regarded as an epitaxial growth of the iPP crystal from the EOR phase. On the contrary, no indication of such epitaxial growth of the iPP crystal lamellae is found in the iPP-EOR9 [Fig. 11(b)].

A number of studies on the compatibility of the blends composed of iPP and ethylenic TPE have been reported so far.[21–25] In these reports, iPP and TPE were miscible (single phase) at higher temperature above the T_m of both components under high shear field such as injection-molding, and then phase-separated via the spinodal decomposition (SD) in a quiescent state during cooling process. The demixing growth rate of the TPE domains, thus the phase-separation rate, was greatly dependent on comonomer contents in the TPE; slow for the TPE blend with higher comonomer contents while fast for the one with lower comonomer contents.[21,25]

Therefore, the morphological difference in the iPP crystal lamellae near the interface region observed

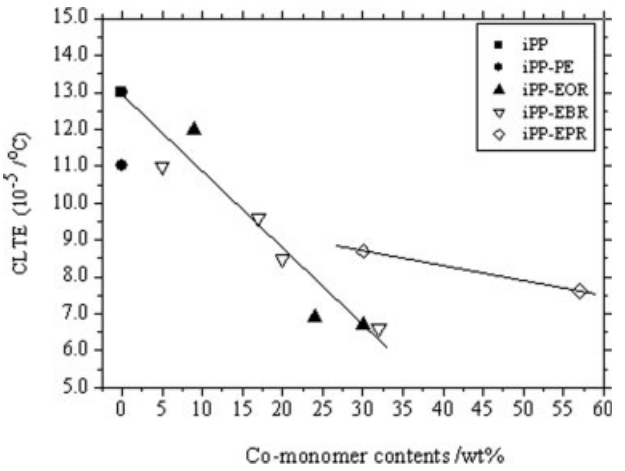

Figure 12 CLTE of the iPP-TPE blends as a function of comonomer contents in the TPE.

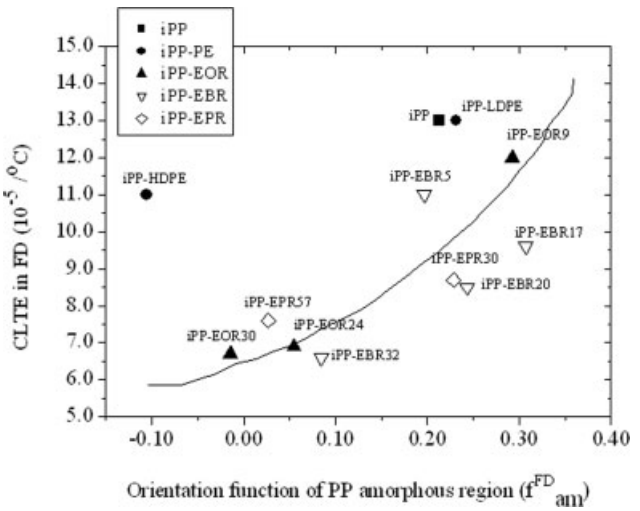

Figure 13 Correlation of the CLTE with the orientation function of the iPP amorphous chains in the blend.

above would be determined by which will complete faster, the phase-separation or the iPP crystallization during cooling process. For the iPP-EOR30, the phase-separation of the iPP amorphous chains from the TPE phase would be arrested by the faster iPP crystallization, and thereby considerable amount of the iPP amorphous chains would be remained inside the TPE phase. On the other hand, for the iPP-EOR9, the iPP amorphous chains would diffuse into the iPP matrix due to the faster phase-separation over the iPP crystallization.

Moreover, the T_m and X_c values of the iPP crystal in the blends reported in Table II are almost comparable to that of plain iPP within experimental errors, irrespective of the polymers as minor components and their comonomer contents. Such a finding indicates that the perfection and thickness of the iPP lamellae in the blends are unaffected by the presence of other olefinic polymers, and thus such polymers do not interfere with the iPP crystallization process in contrast to the iPP amorphous solidification process described earlier.[26]

Correlation of CLTE with type and contents of comonomer in the TPE

Figure 12 shows the average CLTE (α^{obs}) as a function of comonomer content of the combined TPE. All the CLTEs of the blends exhibit smaller values than that in the neat iPP, and decrease linearly with increasing comonomer contents. Note that the CLTE value in the iPP-EOR30 or iPP-EBR32 is ~ 6.0 (10^{-5}/°C). This value is comparable to that in filled iPP-based composites containing 25–30 wt % talc. The CLTE result is practically useful from the view point of the weight reduction of the molded articles so that we can achieve the CLTE decrease without higher density fillers.

In addition, the CLTE of the iPP-EOR30 after passed through an extruder twice and then injection-molded was 6.8 (10^{-5}/°C), comparable to that of the virgin one, exhibiting an excellent recyclablity of this system which can contribute a lot to waste reduction, thus environmental preservation. It should be emphasized as another advantageous point of this system.

Moreover, we examined the CLTE in the case of the injection-molded specimen with less than 3 mm in thickness in order to study the thickness dependence of the CLTE; the CLTE for the injection specimen with 2 mm in thickness using the iPP-EOR30 was 7.0 (10^{-5}/°C), being comparable to that with 3 mm in thickness. It exhibits no thickness dependence of the CLTE in this system. In other words, the blend systems in this study have excellent versatility of applicable molding articles.

As discussed in the previous section (Fig. 11), the comonomer contents in the TPE are deeply associated with the rate of the phase-separation via the SD. Hence, the tendency of the CLTE toward the comonomer contents may also have a high correla-

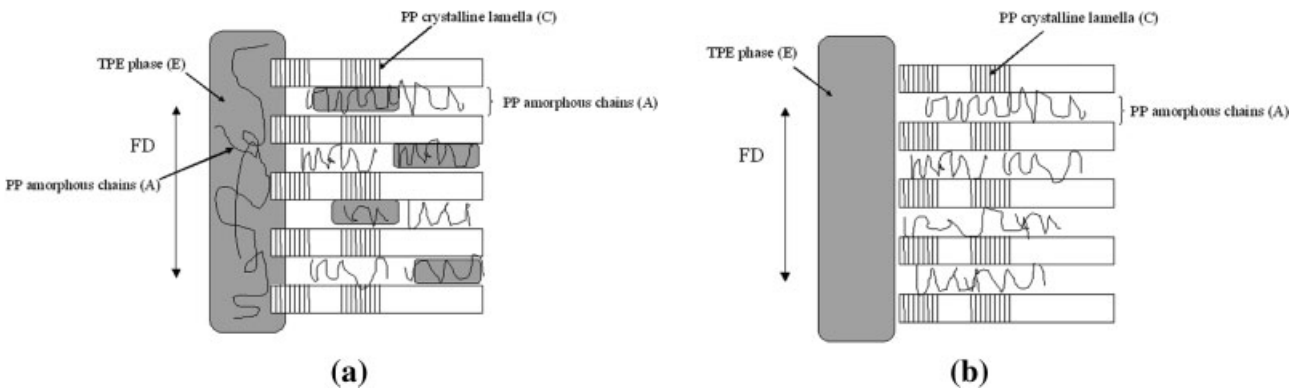

Figure 14 Schematic representation of the difference of the location of the iPP crystalline (C), the iPP amorphous (A), and the TPE (E) region between the blend with higher comonomer contents in the TPE (a) and the lower comonomer contents (b), respectively.

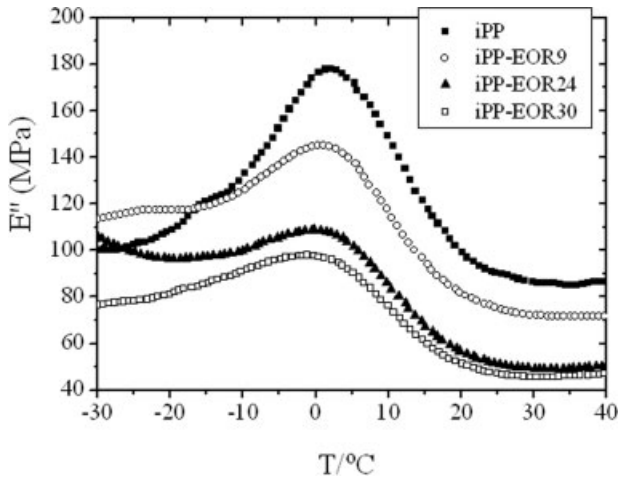

Figure 15 Temperature dependence of loss modulus E'' for the iPP-EOR blend series.

tion with the phase-separation rate; the more the TPE comonomer contents thus the slower the phase-separation, the lower the CLTE.

Moreover, it is found that the CLTEs in the PE, EOR, and EBR blends are on the same straight line irrespective of the difference in the comonomer types whereas the CLTEs in the EPR blends on the another line which exhibits gentler gradient with increase in the comonomer contents. From the schematic representation (Fig. 10), the former blend series and the latter ones had different TPE arrays, the lamella-sheet and the ellipsoidal slab array, respectively. Therefore, the differences in the CLTE sensitivity to the comonomer contents between the EPR blends and other ones are greatly dependent on the difference in the array of the TPE domain. The lamella-sheet array is considered to be more effective for suppressing the CLTE, when compared with the ellipsoidal slab array.

Correlation of CLTE with orientation of the iPP amorphous chains

The CLTE as a function of the orientation function of the iPP amorphous chains, f_{am}^{FD} is shown in Figure 13. The CLTE increases with the f_{am}^{FD}, thus suggesting that the blends with smaller f_{am}^{FD} give the lower CLTE. In addition, the blends with higher comonomer contents in the TPE show the smaller f_{am}^{FD}, almost isotropic ($\sim$ 0). The iPP amorphous chains residing between the interlamella in the iPP matrix are reported to be oriented, forming shish structures even in the core layers upon injection-molding.[27–31] Also, Na et al. reported that shish structures with larger size cannot be transformed to random coil entirely even subjected to annealing at 200°C for 60 min.[31] Hence, most of the shish-like structures in the blends would remain as they are during annealing at 100°C which is much lower than 200°C.

Hence, the isotropic iPP amorphous chains observed in the blend with high comonomer contents would correspond to the ones trapped inside the TPE phase not the ones in the iPP matrix because of the slower phase-separation. Here, the orientation of the iPP amorphous chains inside the TPE phase accompanied by the deformation of the TPE phase could be neglected except for the PE, EOR9, and EBR5 blends because the specimen was annealed at above the T_m of the TPE before evaluation, and thereby the orientation of the iPP amorphous chains would be fully relaxed. In the case of the iPP blends with PE, EOR9, and EBR5 having lower comonomer contents and melting point above 100°C, most of the iPP amorphous chains would be expected to be present in the iPP matrix as pointed out, and thus the orientation of the iPP amorphous chains in the rubbery phase would be small enough to be neglected.

DISCUSSION

In this section, we will discuss the relationship of the CLTE with the variation of comonomer contents of the TPE in the blend from the point of view of the location of iPP amorphous, crystal phase and the TPE phase accompanied by the difference in the phase-separation rate.

On the basis of the morphological and POM results, the morphologies near the interface region corresponding to the blends with higher or lower contents of comonomer in the TPE are schematically shown in Figure 14(a,b), where the relationship of location of each iPP crystalline-(C) , iPP amorphous-(A) and TPE region (E) is demonstrated. The location of the iPP amorphous chains is emphasized as a major difference between the two blends.

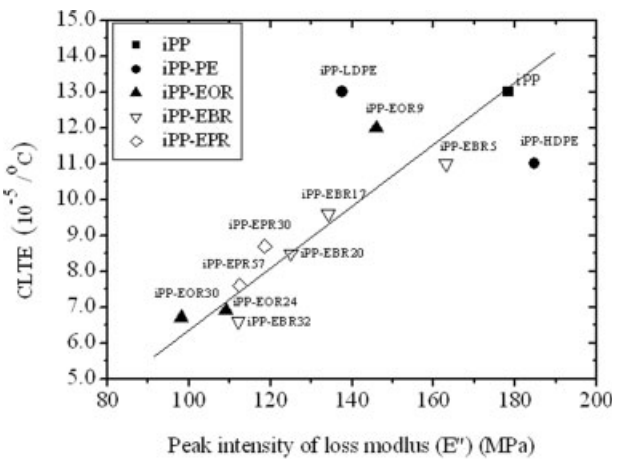

Figure 16 CLTE as a function of the peak intensity of the loss modulus E'' corresponding to the segmental motion of the iPP amorphous chains.

The CLTE of amorphous PP was reported to be 20–30 (10^{-5}/°C),[32] which is comparable to that of the TPE[32] and high enough to have a great influence on the CLTE of the entire blend system, depending on the location of the iPP amorphous chains. The thermal expansion, thus the CLTE, is deeply associated with a segmental motion of a molecular chain by temperature variation. By investigating the peak intensity of the loss modulus (E'') belonging to the α_a relaxation of the iPP amorphous chains obtained by DMTA,[33] we discussed the difference of the segmental motion of the iPP amorphous chains by the change of the location of the iPP amorphous chains.

Figure 15 shows the temperature dependence of E'' for the iPP-EOR blends series. A peak around 0°C belonging to the α_a relaxation of the iPP amorphous chain segment is observed in any blends. As increasing the comonomer contents of EOR in the blend, the corresponding E'' decreased, thus implying the decrease in the mobility of the iPP amorphous chain segment according as the increase in octene contents.

Figure 16 shows the correlation of the peak intensities of E'' around 0°C with the CLTEs for all the blends. Two features are found: the blends with lower CLTE values exhibit lower E'' peak intensities; and the blends with higher contents of comonomer in the TPE show lower E'' peak intensity. These results can be well accounted for by the difference in the mobility of the iPP amorphous chain segment being inside the TPE or between the interlamellae in the matrix; the mobility of the iPP amorphous chains trapped inside the TPE is restricted and low by the rigid iPP crystal lamellae connecting in parallel with the TPE phase, and on the other hand, the mobility of the one between the interlamellae in the matrix is high due to no restriction.

From these consequences, we can assume the plausible mechanism for suppressing the CLTE along FD. In the case of the blend with high comonomer contents in the TPE, considerable amount of the PP amorphous chains would be confined in the softer TPE thus leading to being isotropic, and thereby the thermal expansions of both the TPE and the iPP amorphous chains trapped inside the TPE would be restricted simultaneously by the rigid PP phase. Hence, the CLTEs in FD for this blend series are suppressed to be extremely low.

On the other hand, most of the PP amorphous chains in the low comonomer TPE blend would exist in the interlamella between the iPP crystalline phases, which may still have high CLTE due to little or no mechanical constraint.

CONCLUSIONS

In the injection-molded blends consisting of iPP and various types of ethylenic TPE with different comonomer contents, it was found that the CLTE values in FD decreased with the increase in the comonomer contents in the TPE. The CLTE value was greatly dependent on both the arrays of the TPE domains and the comonomer contents. The lamella-like sheet array in the TPE was more sensitive to the change in the comonomer contents relative to the slab array. The differences in the comonomer contents in the TPE among the blends were associated with the rate of the phase separation via the SD; slow for the blend with higher comonomer contents in the TPE and fast for the one with lower comonomer contents. Therefore, in the case of the blend with higher comonomer contents in the TPE, considerable amount of the iPP amorphous chains was remained trapped inside the TPE domain as a result of slower phase separation arrested by faster iPP crystallization. The extremely low CLTE observed in the blend with higher comonomer contents in the TPE could be explained as a result of simultaneous suppression of thermal expansion of both the TPE and the iPP amorphous chains which were responsible for enhancing the CLTE of the entire blend system.

References

1. Moore, E. P., Jr. Polypropylene Handbook; Carl Hanser Verlag: Münich, 1996.
2. Bradrup, J.; Immergut, E. H. Polymer Handbook, 3rd ed.; Wiley: New York, NY, 1989.
3. Ushigi, H.; Saito, T.; Hashitani, T. Kagaku Binran Kisohen II; Maruzen: Tokyo, 1993.
4. Yoon, P. J.; Fornes, T. D. Polymer 2002, 43, 6727.
5. Felthan, S. J.; Bates, B. J. J Mater Sci 1972, 7, 2309.
6. Holliday, L.; Robinson, J. J Mater Sci 1973, 8, 301.
7. Thomason, J. L.; Groenewoud, W. M. Compos A 1996, 27, 555.
8. Ono, M.; Washiyama, J.; Nakajima, K.; Nishi, T. Polym J 2004, 36, 563.
9. Ono, M.; Washiyama, J.; Nakajima, K.; Nishi, T. Polymer 2005, 46, 4899.
10. Ono, M.; Nakajima, K.; Nishi, T. Kautschuk Gummi Kunstsoffe 2006, 11, 574.
11. Wu, G.; Nishida, K.; Takagi, K.; Sano, H.; Yui, H. Polymer 2004, 5, 3085.
12. Wilchinsky, W. J Appl Polym Sci 1963, 7, 923.
13. Kunugi, T.; Ito, T.; Hashimoto, M.; Ooishi, M. J Appl Polym Sci 1983, 28, 179
14. Suzuki, A.; Sugimura, T.; Kunugi, T. J Appl Polym Sci 2001, 81, 600.
15. Taylor, G. I. Proc R Soc London Ser A 1934, 134, 501.
16. Cox, R. G. J Fluid Mech 1969, 37, 601.
17. Tomotika, S.; Cox, R.; Mason, S. G. J Colloid Sci 1972, 38, 395.
18. Kim, B. K.; Do, H. I. J Appl Polym Sci 1996, 60, 2207.
19. Vadas, E. B.; Goldsmith, H. L.; Mason, S. G. Trans Soc Rheol 1976, 20, 373.
20. Han, C. D.; Kim, Y. W. Trans Soc Rheol 1975, 19, 245.
21. Sano, H.; Matsuda, M.; Sato, H.; Nomura, T. Kobunshi Ronbunshu 1999, 56, 693.
22. Inaba, N.; Sato, K.; Suzuki, S.; Hashimoto, T. Macromolecules 1986, 19, 1690.
23. Inaba, N.; Yamada, T.; Suzuki, S.; Hashimoto, T. Macromolecules 1988, 21, 407.
24. Lim, S. W.; Lee, K. H.; Lee, C. H. Polymer 1999, 40, 2837.

25. Lee, J. K.; Lee, J. H.; Lee, K. L.; Jin, B. S. J Appl Polym Sci 2000, 81, 695.
26. D'Orazio, L.; Mncarella, C.; Martuscelli, E.; Sticotti, G.; Massari, P. Polymer 1993, 34, 3671.
27. Wang, Y.; Na, B.; Fu, Q.; Men, Y. Polymer 2004, 45, 207.
28. Kumaraswamy, G.; Kornfield, J. A.; Yeh, F.; Hsiao, B. S. Macromolecules 2002, 35, 1762.
29. Seki, M.; Thurman, D. W.; Oberhauser, J. P.; Kornfield, J. A. Macromolecules 2002, 35, 2583.
30. Kumaraswamy, G.; Verma, R. K.; Issaian, A. M.; Wang, P.; Kornfield, J. A.; Yeh, F.; Hsiao, B. S.; Olley, R. H. Polymer 2000, 41, 8931.
31. Na, B.; Wang, Y.; Zhang Q.; Fu, Q. Polymer 2004, 45, 6245.
32. Zoller, P.; Walsh, D. J. Standard Pressure-Volume-Temperature Data for Polymers; Technomic Publishing, 1995.
33. Takayanagi, M.; Imada, K.; Kajiyama, T. J Polym Sci C 1966, 15, 263.